

What to expect: kilonova light curve predictions via equation of state marginalization

Andrew Toivonen¹*, Gargi Mansingh^{1,2,3}, Holton Griffin¹, Armita Kazemi¹, Frank Kerkow¹, Stephen K. Mahanty¹, Jacob Markus¹, Seiya Tsukamoto¹, Sushant Sharma Chaudhary⁴, Sarah Antier⁵, Michael W. Coughlin¹, Deep Chatterjee⁶, Reed Essick⁷, Shaon Ghosh⁸, Tim Dietrich^{9,10}, Philippe Landry⁷

¹School of Physics and Astronomy, University of Minnesota, Minneapolis, Minnesota 55455, USA

²Department of Physics, American University, 3501 Nebraska Ave NW, Washington, DC 20016

³Nicholas & Lee Begovich Center for Gravitational-Wave Physics & Astronomy, California State University, Fullerton, 800 N State College Blvd, Fullerton, CA 92831

⁴Institute of Multi-messenger Astrophysics and Cosmology, Missouri University of Science and Technology, Physics Building, 1315 N. Pine St., Rolla, MO 65409, USA

⁵Observatoire de la Côte d'Azur, Université Côte d'Azur, Boulevard de l'Observatoire, 06304 Nice, France

⁶MIT Kavli Institute for Astrophysics and Space Research 77 Massachusetts Avenue, McNair Building (MIT Building 37) Cambridge, MA 02139

⁷Canadian Institute for Theoretical Astrophysics, 60 St. George St, Toronto, Ontario M5S 3H8, Canada

⁸Montclair State University, 1 Normal Ave, Montclair, NJ 07043

⁹Institut für Physik und Astronomie, Universität Potsdam, Haus 28, Karl-Liebknecht-Strasse 24/25, 14476, Potsdam, Germany

¹⁰Max Planck Institute for Gravitational Physics (Albert Einstein Institute), Am Mühlenberg 1, Potsdam 14476, Germany

Accepted XXX. Received YYY; in original form ZZZ

ABSTRACT

Efficient multi-messenger observations of gravitational-wave candidates from compact binary coalescence (CBC) candidate events relies on data products reported in low-latency by the International Gravitational-wave Network (IGWN). While data products such as `HasNS`, the probability of at least one neutron star, and `HasRemnant`, the probability of remnant matter forming after merger, exist, these are not direct observables for a potential kilonova. Here, we present new kilonova light curve and ejecta mass data products derived from merger quantities measured in low latency, by marginalizing over our uncertainty in our understanding of the neutron star equation of state (EoS) and using measurements of the source properties of the merger, including masses and spins. Two additional types of data products are proposed. The first is the probability of a candidate event having mass ejecta (m_{ej}) greater than $10^{-3} M_{\odot}$, which we denote as `HasEjecta`. The second are m_{ej} estimates and accompanying `ugrizy` and `HJK` kilonova light curves predictions produced from a surrogate model trained on a grid of kilonova light curves from POSSIS, a time-dependent, three-dimensional Monte Carlo radiative transfer code. We are developing this data products in the context of the IGWN low-latency alert infrastructure, and will be advocating for their use and release for future detections.

Key words: gravitational waves, kilonova – methods: statistical

1 INTRODUCTION

The combined detection of the kilonova AT2017gfo (Coulter et al. 2017; Smartt et al. 2017b; Abbott et al. 2017c) and gravitational-wave (GW) observations resulting from the binary neutron star merger GW170817 (Abbott et al. 2017b) has led to immense interest in the field of multi-messenger astrophysics. Kilonovae are short lived astrophysical transients that may result from either binary neutron star (BNS), or a neutron star-black hole (NSBH) mergers and are of particular astrophysical interest due to the fact that kilonovae

are expected to be sites of r-process nucleosynthesis, through which it is theorized heavy elements can be produced. The radioactive decay and interactions of these r-process elements are what powers the kilonova emission we hope to observe (Lattimer & Schramm 1974; Li & Paczynski 1998; Metzger et al. 2010; Kasen et al. 2017b). While GW170817 led to breakthroughs in nuclear astrophysics (Margutti et al. 2017; Smartt et al. 2017a; Kasliwal et al. 2017; Kasen et al. 2017a; Watson et al. 2019), cosmology (Abbott et al. 2017a; Coughlin et al. 2020; Dietrich et al. 2020), and tests of General Relativity (Ezquiaga & Zumalacárcel 2017; Baker et al. 2017; Creminelli & Vernizzi 2017), much remains to be learned about these rare events, including the diversity of their intrinsic

* E-mail: toivo032@umn.edu

2 *Toivonen et al.*

parameters, their emission, and the heavy elements produced by r-process nucleosynthesis in these mergers.

Advanced LIGO (aLIGO)'s (Aasi et al 2015), Advanced Virgo (AdVirgo)'s (Acernese et al 2015) and KAGRA's (Akutsu et al. 2021) fourth observing run (O4) is underway as of May 23, 2023¹, and the search for gravitational wave events and their counterparts (Abbott et al. 2020a) has resumed. Searches for kilonovae are challenging due to the fact that they are short lived events, can be relatively faint, and may not be well localized. Sky localizations for gravitational wave events can span $\approx 100 - 10,000$ deg² (Röver et al. 2007; Fairhurst 2009; Fairhurst 2011; Grover et al. 2014; Wen & Chen 2010; Sidery et al. 2014; Singer et al. 2014; Berry et al. 2015; Essick et al. 2015; Cornish & Littenberg 2015; Klimenko et al. 2016). However, in spite of these challenges, it is imperative to locate the transient as quickly as possible in the hope of observing the peak of emissions. A number of wide-field survey telescopes are used to try and cover these large sky localizations, such as: the Panoramic Survey Telescope and Rapid Response System (Pan-STARRS) (Morgan et al. 2012), Asteroid Terrestrial-impact Last Alert System (ATLAS) (Tonry et al. 2018), the Zwicky Transient Facility (ZTF) (Bellm et al. 2018; Graham et al. 2019; Ahumada et al. 2024), and in the near future BlackGEM (Bloemen et al. 2015), the Large Synoptic Survey Telescope (LSST) (?), the Nancy Grace Roman Space Telescope² (Andreoni et al. 2024), and Ultraviolet Explorer (UVEX) (Kulkarni et al. 2021). While GW170817 is the only CBC merger event that has provided us with joint observations of a GW signal, kilonova, and short gamma-ray burst (sGRB), it is also potentially possible to identify kilonovae associated with sGRBs (Tanvir et al. 2013; Ascenzi et al. 2019; Jin et al. 2020; Rastinejad et al. 2022), or even serendipitously in survey operations (Andreoni et al. 2021; Almualla et al. 2021).

These searches are aided by source classification efforts, which we can use to determine the origin of gravitational wave (GW) events (Chatterjee et al. 2020; Berbel et al. 2024). In addition, there have been multiple efforts to simulate GW detections and constrain rates for O4 and beyond Petrov et al. (2022); Colombo et al. (2022); Kien drebeogo et al. (2023). With O4 underway, we hope for additional BNS detections and follow-up opportunities. These observing scenarios simulations tell us what we can expect to observe, and can even help us constrain poorly measured parameters, like the inclination angle, as discussed in Sec. 2.5. The parameters of the binary before merger, such as the mass ratio and the masses of the objects involved, along with the EoS, can help predict the mass ejected from the merger and the light curves associated with a possible kilonova (Bauswein et al. 2013; Piran et al. 2013; Abbott et al. 2017b; Bauswein et al. 2017; Dietrich & Ujevic 2017; Radice et al. 2018). The relationship between light curves and binary parameters can also be used to place constraints on the character of the progenitor systems and the mass ejected (Coughlin et al. 2017; Smartt et al. 2017b; Coughlin et al. 2018; Bulla 2023).

Predicting whether we can expect to see a kilonova, how bright that kilonova may be, and where it will be localized in the sky are all crucial for astronomers who work on follow-up of GW events. Currently, the sky localization is provided through sky maps, produced by BAYESTAR (Singer & Price 2016) and Bilby (Ashton et al. 2019). These efforts are intended to allow for more informed and efficient follow-up searches. There are also existing properties, HasNs and HasRemnant (Chatterjee et al. 2020), which are provided by

the EM-bright pipeline and encode the probability that there will be at least one neutron star (NS) and non-zero m_{ej} , respectively, by providing estimates of the amount of m_{ej} produced and the M_{AB} of the kilonova.

In this paper, we propose two new data products, focused on observable properties directly tied to kilonovae, partially building on the work of (Stachie et al. 2021). We use similar ejecta fits and also define a quantity HasEjecta to describe the likelihood of having a significant amount of m_{ej} . One noticeable difference is our focus on using parameter estimation, instead of template based estimates. The first data product is the probability of a candidate event having m_{ej} greater than $10^{-3} M_{\odot}$; we denote this quantity as HasEjecta. This quantity is useful for establishing the likelihood of a kilonova counterpart, regardless of brightness. The $10^{-3} M_{\odot}$ cutoff was chosen for three reasons, (i) our kilonova surrogate models were not trained on grid points below this value, (ii) ejecta fits can have large uncertainties that dominate at low values, and (iii) this provides a reasonable floor estimate for the total m_{ej} capable of producing an observable kilonova. To directly support electromagnetic counterpart searches, we also propose to provide predicted $ugrizy$ and HJK light curves. To do so, we use a surrogate model based on the time-dependent, three-dimensional Monte Carlo radiative transfer code POSSIS (Bulla 2019). Using POSSIS, we produce kilonova light curves by simulating packets of photons released by the radioactive decay of r-process nuclei in a kilonova. POSSIS takes input in the form of a model that defines densities, compositions, and geometry of the ejecta, and outputs light curves and spectra as a function of inclination angle. POSSIS simulations are computationally expensive, so a grid of kilonova light curves are computed and then used to train a surrogate light curve model with The Nuclear Multimessenger Astronomy Framework (NMMA)³ (Pang et al. 2023). NMMA is a nuclear physics and cosmology library used for analysis of BNS and NSBH systems, as well as potential counterparts. To create the light curve model, NMMA starts with a grid of POSSIS simulations across input parameters, and uses a neural network to interpolate between that grid and generalize to arbitrary parameters. For this work, we use the light curve model referred to as Bu2019lm (Bulla 2019), which depends on the dynamical mass ejecta ($m_{\text{ej}}^{\text{dyn}}$), wind ejecta $m_{\text{ej}}^{\text{wind}}$, inclination angle (θ), and the opening angle ϕ , as will be discussed more later on.

Sec. 2 provides the workflow for producing the proposed data products from what is available in low latency from IGWN searches. We present performance for the proposed data products in Sec. 3, while Sec. 4 provides our conclusions and plans for future research.

2 MODELING

2.1 Workflow overview

Fig.1 provides an overview of the workflow of our kilonova ejecta and light curve predictions. We start with a GW detection by one of the CBC searches, and then use initial mass and spin estimates from either the point estimate, or parameter estimation, as discussed in Sec. 2.2. The point estimate has high uncertainties, but is also available in low-latency at the time the alert is sent out. Parameter estimation is more accurate, and covers a range of mass and spin values, but is not available until \sim hours after merger. From there, we

¹ <https://observing.docs.ligo.org/plan>

² <https://roman.gsfc.nasa.gov/>

³ <https://github.com/nuclear-multimessenger-astronomy/nmma>

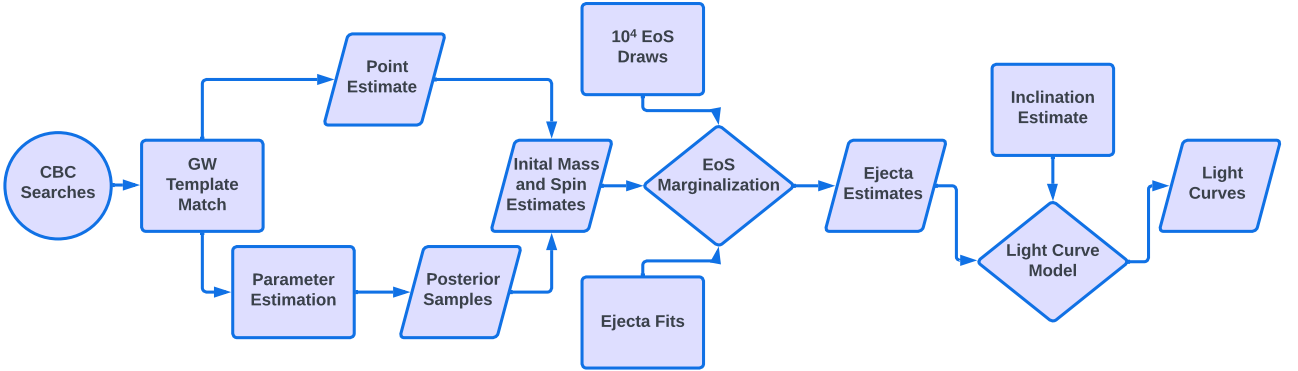


Figure 1. Workflow for the light curve and ejecta mass data products. We start with initial mass and spin estimates from a GW candidate as input, then marginalize over a number of EoS realizations per sample and apply mass ejecta fits. Finally, we use our light curve model to calculate light curves after drawing inclination angles if needed.

marginalize over EoS realizations and use the ejecta fits covered in Sec. 2.4 to calculate the m_{ej} . Each sample is run with a set number of random EoS realizations to effectively cover the parameter space. Finally, adding in an inclination distribution and opening angle, covered in Sec. 2.5 and using our kilonova model covered in Sec. 2.6, we generate kilonova light curves.

2.2 Chirp mass and mass ratio

The chirp mass and mass ratio of a compact object merger are important quantities for characterization of a merger event. The chirp mass is the simplest merger quantity to measure from a GW signal, due to its relationship with the frequency evolution of the signal. Chirp mass, m_{chirp} , is defined as:

$$m_{\text{chirp}} = \frac{(m_1 m_2)^{3/5}}{(m_1 + m_2)^{1/5}} \quad (1)$$

where m_1 is the primary, or larger, mass, while m_2 , the secondary, or smaller, mass. The mass ratio, q , is much more difficult to measure accurately from GW data, and is the ratio between the component masses.

$$q = \frac{m_2}{m_1} \quad (2)$$

Estimates of the q can be made using the phase of the GW signal, but they include significant error. The chirp mass is recovered quite accurately by parameter estimation in most cases, however, there may still be a wide range of possible component mass values due to the poorly constrained mass ratios, meaning the source classification cannot always be clearly ascertained.

We have two possible options for our initial mass and spin estimates: (i) the mass estimates produced by Bilby (Ashton et al. 2019), an automated Bayesian parameter estimation analysis library, and (ii) the point estimate from the CBC template match, e.g. GstLAL (Messick et al. 2017; Tsukada et al. 2023; Ewing et al. 2023), MBTA (Andres et al. 2022), PyCBC (Nitz et al. 2018; Dal Canton et al. 2021), SPIIR (Luan et al. 2012; Hooper et al. 2012). While parameter estimation is the starting point with the most precise measurements, given it provides (i) the most accurate estimate of the true source parameters and (ii) uncertainties, it takes \sim hours to be completed post-merger. If a low-latency prediction is desired,

as may benefit searches for counterparts in the hours after merger, we must use the point estimate as a starting point. There are also promising prospects of real-time machine learning based parameter estimation, which may be available in the future (Dax et al. 2021), but for now we must rely on the point estimate. In this case, we can use the point estimate, or take the chirp mass from the point estimate and draw a mass ratio consistent with that chirp mass value from population level distributions (Coughlin et al. 2022; Kien-drebeogo et al. 2023) informed by GWTC-3 catalogue fits (Abbott et al. 2023). From this chirp mass and mass ratio, we compute the component masses that will be inputs for the simulated ejecta quantities and light curves (see below). For the analysis of Mock Data Challenge (MDC) (Chaudhary et al. 2024) events to follow, we use parameter estimation as the starting point for the reasons outlined above.

2.3 Equation of state and spin distributions

The NS EoS impacts the amount of mass expected to be ejected from a CBC merger as it influences how the NS is tidally disrupted. While the NS EoS remains unknown, there are certain popular EoS in the literature useful for comparisons. In the following, when we need a single EoS to compare to, we will use the SLy (Chabanat et al. 1998) EoS for comparisons to our marginalized range of predictions. This is to provide a singular point of reference for comparison, and to ensure that our predictions are reasonable. The SLy EoS was chosen as it has support from mass-radius posteriors from GW170817 (Abbott et al. 2018).

Within our pipeline, due to the uncertainty in our understanding of the NS EoS, we marginalize over a number of EoS realizations per sample in order to produce our ejecta estimates. For each component mass pair, we draw a specified number of EoS realizations from a set of 10^4 equally weighted EoS realizations in order to cover the parameter space. The EoS realizations are drawn from a Gaussian-process posterior (Legred et al. 2021, 2022) conditioned on a radio pulsar mass measurement (Zhao 2015) and gravitational-wave mass and tidal deformability measurements (Abbott et al. 2017b; Abbott et al. 2020b). For the purpose of our workflow, each sample is run with a different subset but same number of EoS realizations. This number of realizations is a variable within the workflow and can be set as desired. To establish the number sufficient for consistent

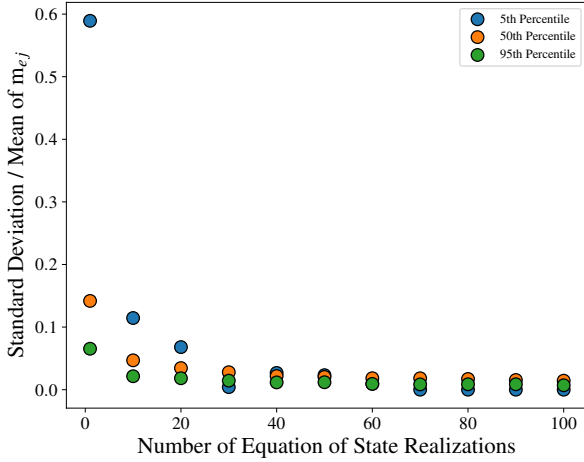


Figure 2. Comparison of relative error between 100 realizations of predictions based on parameter estimation for a single MDC event as a function of the number of EoS realizations per sample. We find that the error falls off asymptotically as the number of EoS realizations increasing, and that there are diminishing returns past 50 EoS realizations, where the error is less than a few percent.

results, we ran a series of tests; Fig. 2 shows how the relative error, defined here as the standard deviation over the median m_{ej} , varies for different numbers of EoS realizations. The standard deviation and mean was found across 100 realizations of the predictions for each number of EoS realizations. We find that 50 EoS realizations reduces the error to less than a few percent, giving us more than sufficient consistency between runs while still being computationally feasible. Beyond this point improvements are negligible. 50 EoS realizations also ensures that even in the case where only a small fraction of the posterior samples produce significant amounts of m_{ej} , we will still adequately cover the parameter space. If running on a point estimate or similar small sample size, all 10^4 samples can be employed.

The NS and black hole (BH) spins may also impact the amount of m_{ej} . As will be covered in Sec. 2.4, the BNS ejecta fits employed do not depend on spin, while the NSBH depend on the total effective spin χ_{eff} :

$$\chi_{\text{eff}} = \frac{\chi_{1,z}/m_1 + \chi_{2,z}/m_2}{m_1 + m_2} \quad (3)$$

This means that our data products will be unchanged by varying spin values for BNS events but impacted for NSBH events. For simulated events from the MDC that we will compare to in Sec. 3, the spin distributions are injected uniform in magnitude and isotropic in orientation, with magnitudes up to 0.4 and 1 for NS and BH respectively (Chaudhary et al. 2024). Just as for candidate GW events, parameter estimation provides spin estimates alongside the component masses, which can then be used for ejecta predictions.

2.4 Dynamical and disk wind ejecta from fits: BNS and NSBH

Having covered the initial merger parameters, we shift our focus to the resulting merger products. The total m_{ej} is calculated in two components: the dynamical ejecta, $m_{\text{ej}}^{\text{dyn}}$, and the disk wind ejecta,

$m_{\text{ej}}^{\text{wind}}$. The first component, $m_{\text{ej}}^{\text{dyn}}$ is produced as the extreme tidal forces of the inspiral tidally deforms and rips mass from a neutron star (Metzger 2017). The other, $m_{\text{ej}}^{\text{wind}}$, is produced by matter that is ejected from the accretion disk of the merger by energetic outflows of particles, sometimes referred to as particle “winds” (Metzger 2017). Estimates of m_{ej} are found from fit by combining the source properties with the EoS used. The EoS provides tables of mass, radius, and tidal deformability information (Legred et al. 2022) which can be used to determine compactness needed for the fits. When making predictions, it is possible to (i) marginalize over EoS in order to effectively cover the uncertainty in this parameter space, or (ii) pick a single named EoS as input. Regardless of the EoS, we use ejecta fits in order to calculate both the dynamical and disk wind ejecta, which are found from separate fits for BNS mergers and NSBH mergers. These are found in Eqs. 4–11 below. We use the fits as implemented in NMMA (Pang et al. 2023).

Moving onto the specific details of the calculations, the total m_{ej} is defined by Dietrich et al. (2020) in Eq. 4, where M_{disk} is the mass of the disk and ζ is the fraction of mass that becomes unbound from the system. Therefore ζM_{disk} is the disk wind ejecta: $m_{\text{ej}}^{\text{wind}}$. We use $\zeta = 0.30$ for both BNS and NSBH mergers (Fernández et al. (2014); Christie et al. (2019); Siegel & Metzger (2018); Fernández et al. (2018)). The total m_{ej} is then simply the sum of the contributions from the $m_{\text{ej}}^{\text{dyn}}$ and $m_{\text{ej}}^{\text{wind}}$ components.

$$m_{\text{ej}} = M_{\text{ej}}^{\text{dyn}} + \zeta M_{\text{disk}} \quad (4)$$

For BNS mergers, we use the following fit in Eq. 5 from (Krüger & Foucart 2020) for $m_{\text{ej}}^{\text{dyn}}$:

$$\frac{M_{\text{ej}}^{\text{dyn}}}{10^{-3} M_{\odot}} = \max \left(0, \left[\frac{a}{C_1} + b + \left(\frac{m_1}{m_2} \right)^n + c C_1 \right] + [1 \leftrightarrow 2] \right) \quad (5)$$

In these expressions, m_1 is the mass of the primary, or largest component mass, while m_2 is the secondary, or smaller mass. For BNS both are neutron stars, while for NSBH m_1 is always the black hole, while m_2 is the neutron star. In the same way, C_1 is the compactness of the primary mass, while C_2 is the compactness of the secondary. From the fit, the coefficients are: $a = -9.335$, $b = 114.17$, $c = -337.56$, and $n = 1.5465$. The term $[1 \leftrightarrow 2]$ simply refers to an addition of the same terms with indices swapped.

Then, for $m_{\text{ej}}^{\text{wind}}$, again for BNS mergers, we use the following in Eq. 6 from Dietrich et al. (2020):

$$\log_{10} \frac{M_{\text{disk}}}{M_{\odot}} = \max \left(-3, a \left(1 + b \tanh \left(\frac{c - m_{\text{tot}}/M_{\text{threshold}}}{d} \right) \right) \right) \quad (6)$$

where a and b are given by

$$a = a_o + \delta a \cdot \xi, \quad b = b_o + \delta b \cdot \xi, \quad (7)$$

and a_o , b_o , δa , δb , c , and d are all free parameters. The parameter ξ is given by

$$\xi = \frac{1}{2} \tanh (\beta (q - q_{\text{trans}})), \quad (8)$$

where β and q_{trans} are free parameters and $q \equiv m_2/m_1 \leq 1$ is defined as the mass ratio. The best-fit model parameters are $a_o = -1.581$, $\delta a = -2.439$, $b_o = -0.538$, $\delta b = -0.406$, $c = 0.953$, $d = 0.0417$, $\beta = 3.910$, $q_{\text{trans}} = 0.900$. The threshold mass

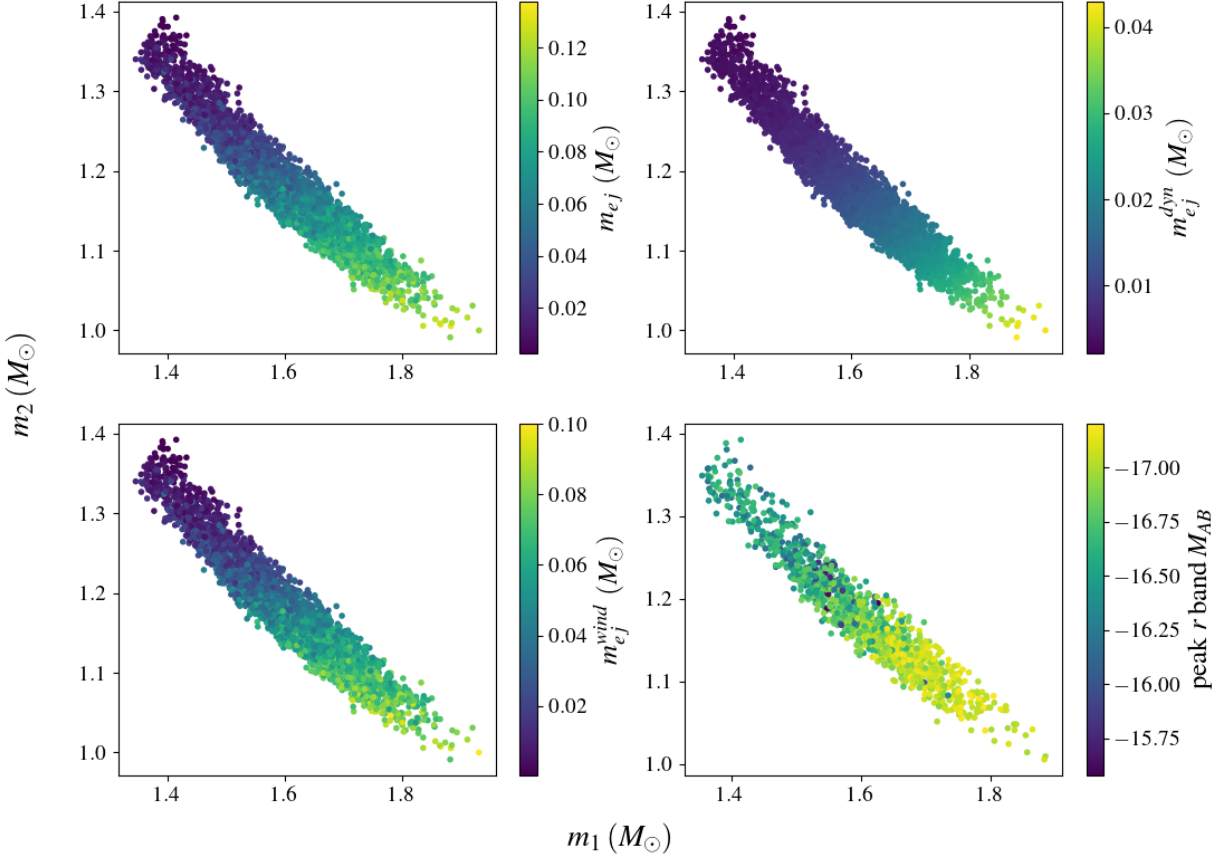


Figure 3. Scatter plots of m_{ej} and light curve predictions using EoS marginalization and parameter estimation from a $m_1 = 1.40M_{\odot}$, $m_2 = 1.34M_{\odot}$ injection. On the upper left we have m_{ej} , upper right $m_{\text{ej}}^{\text{dyn}}$, lower left $m_{\text{ej}}^{\text{wind}}$, and on the lower right the peak r -band M_{AB} . We see a strong correlation between all four quantities with some slight variations.

$M_{\text{threshold}}$ for a given EoS is estimated by the following (Agathos et al. 2020):

$$M_{\text{threshold}} = \left(2.38 - 3.606 \frac{M_{\text{TOV}}}{R_{1.6}} \right) M_{\text{TOV}}, \quad (9)$$

where M_{TOV} is the maximum mass of a non-spinning NS and and $R_{1.6}$ is the radius of a $1.6M_{\odot}$ NS.

Now moving to NSBH mergers, we use the $m_{\text{ej}}^{\text{dyn}}$ fit from Krüger & Foucart (2020), shown in Eq. 10.

$$M_{\text{dyn}}(M_{\odot}) = m_2^{\text{bar}} \left(a_1 \left(\frac{m_1}{m_2} \right)^{n_1} \frac{1 - 2C_2}{C_2} - a_2 \left(\frac{m_1}{m_2} \right)^{n_2} \frac{r_{\text{ISCO}}}{m_1} + a_4 \right) \quad (10)$$

The coefficients are: $a_1 = 0.007116$, $a_2 = 0.001436$, $a_4 = -0.02762$, $n_1 = 0.8636$, and $n_2 = 1.6840$.

Again for NSBH, the $m_{\text{ej}}^{\text{wind}}$ fit is defined by Foucart et al. (2018) here in Eq. 11.

$$M_{\text{disk}}(M_{\odot}) = m_2^{\text{bar}} \max \left(0, \alpha \frac{1 - 2C_2}{\eta^{1/3}} - \beta r_{\text{ISCO}} \frac{C_2}{\eta} + \gamma \right)^{\delta} \quad (11)$$

In Eq. 11, m_2^{bar} refers to the baryonic mass of the secondary mass, η is the reduced mass and is defined as $\eta = (m_1 m_2) / (m_1 + m_2)$, and r_{ISCO} is the innermost stable circular orbit of the binary. From the fit, the coefficients are: $\alpha = 0.4064$, $\beta = 0.1388$, $\gamma = 0.2551$, and $\delta = 1.7612$.

Predicted distributions of m_{ej} , $m_{\text{ej}}^{\text{wind}}$, and $m_{\text{ej}}^{\text{dyn}}$ using these fits and marginalizing over EoS can be seen in Fig. 3 for a MDC event with injected masses of $m_1 = 1.40M_{\odot}$, $m_2 = 1.34M_{\odot}$. Further discussion found in Sec. 3.3.

2.5 Inclination

The mass ejected from a neutron star is not thought to be perfectly uniform and spherical (Heinzel et al. 2021; Sneppen et al. 2023), which means the electromagnetic (EM) emission from a kilonova will not be isotropic. We expect to observe brighter emissions for face-on events, meaning $\theta \simeq 0^{\circ}$. In the case of kilonovae, this inclination angle, θ , also known as the viewing angle, ranges from 0 to 90° as it is equivalent from 90 to 180° due to symmetry; in the GW case, face-on vs. face-off can be differentiated, and therefore measurements are reported from 0 to 180° . Observationally, we would

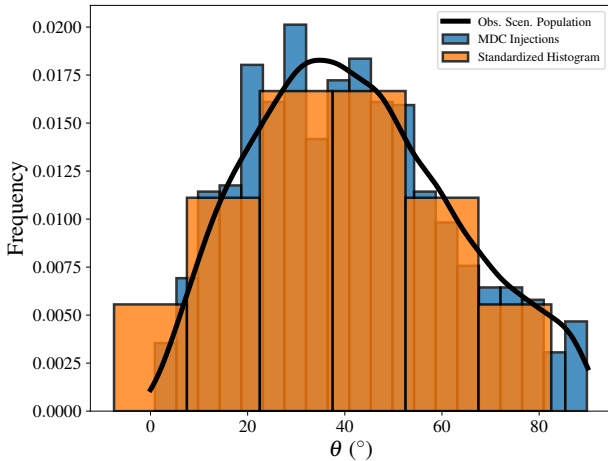


Figure 4. The two methods available for drawing θ : the observing scenarios population distribution (Coughlin et al. 2022) (black) and a standardized histogram (orange), compared to the histogram of θ from MDC injection samples with predicted $m_{\text{ej}} \geq 10^{-3} M_{\odot}$ (blue). When using the observing scenarios distribution we draw a sample from the KDE for each initial component mass sample provided. When using the standardized histogram method, each initial component mass sample is run with $\theta = [0, 15, 30, 45, 60, 75]$ with counts proportional to the histogram, meaning each sample is run with the same θ values for consistency even with small sample sizes.

expect to see an θ distribution that is uniformly distributed in the projection along the line of sight, $(\cos \theta)$. However, because GW's have higher amplitudes for face-on events, we are in fact biased towards those face-on events, as those events will be louder and more likely to be detected. Taking both these factors into account, we will get a distribution that peaks at lower θ values and tails off toward higher θ values, as seen in Fig. 4.

In the workflow, we have two means for drawing θ . The first is shown by the black line in Fig. 4. This shows the θ distribution resulting from observing scenarios simulations (Coughlin et al. 2022; Kiendrebeogo et al. 2023); these are based on GWTC-3 (Abbott et al. 2023) catalog fits which are simulated using Bayestar (Singer & Price 2016), which simulates the matched filtering process and Gaussian noise in order to mimic realistic GW detections. Fig. 4 shows the KDE that estimates the θ distribution based on those simulations, and we can sample from this distribution. The second method uses standardized draws to mimic that same distribution, but instead of providing one random value, this method covers a range of θ values. For each sample, we cover the values 0, 15, 30, 45, 60, and 75 with probabilities proportional to what is seen in Fig. 4. This method removes the random nature of the draws which can be useful for small sample sizes. These two methods converge for large sample sizes and can be chosen based on the sample size and any time or resource constraints.

2.6 Kilonova light curve model

Our kilonova light curve model is based on the time-dependent, three-dimensional Monte Carlo radiative transfer code POSSIS (Bulla 2019), which can simulate kilonova light curves for a range of input parameters. A grid of these simulated kilonovae is then used to train a model in NMMA in order to generalize predictions to arbitrary

parameters. The model takes parameters of inclination angle (θ), half-opening angle (ϕ), dynamical ejecta $m_{\text{ej}}^{\text{dyn}}$, and wind ejecta $m_{\text{ej}}^{\text{wind}}$, and outputs light curves in nine *ugrizy* and *HJK* absolute magnitude (M_{AB}) bands. For this analysis, we have fixed this half-opening angle value to 30° , which was shown to be a reasonable fit to GW170817 (Pang et al. 2023).

Fig. 3 shows a peak *r* band M_{AB} light curve predictions from a single simulated event with $m_1 = 1.40 M_{\odot}$ and $m_2 = 1.34 M_{\odot}$, and the associated m_{ej} distributions. Fig. 5 shows all light curves across nine bands for that same event, as well as the median and 90% credible interval for m_{ej} and M_{AB} . The right panel of Fig. 7 shows peak *r*-band M_{AB} across a range of component masses consistent with BNS and NSBH mergers. The points show the median value across EoS realizations. In general, we find low mass BNS events produce the brightest events, and M_{AB} is strongly correlated with m_{ej} . The light curve data products will be covered in detail and analyzed in Sec. 3.

3 ANALYSIS OF DATA PRODUCTS

3.1 Proposed data products

The first of our data products consists of three categories, which sum to a probability of 1: `BNS_ejecta`, `NSBH_ejecta`, and `no_ejecta`. `BNS_ejecta` refers to the probability that there will be significant m_{ej} , defined as greater than $10^{-3} M_{\odot}$, produced by a BNS merger. Similarly, `NSBH_ejecta` refers to the probability that there will be significant m_{ej} produced by a NSBH merger; finally, `no_ejecta` refers to the probability that there will be $m_{\text{ej}} < 10^{-3} M_{\odot}$. Each of these quantities assume the event is astrophysical in nature, and `no_ejecta` is indiscriminate of the type of merger. Due to EoS and parameter uncertainties, it is possible for predictions to contain non-zero values for both `BNS_ejecta` and `NSBH_ejecta`. Given EoS realizations define the maximum mass of the neutron star, a sample near the border of a neutron star or black hole may have individual EoS realizations classifying the object nature differently. The sum of `BNS_ejecta` and `NSBH_ejecta` will then provide the probability that a given event has significant ejecta, i.e. greater than $10^{-3} M_{\odot}$. We denote this quantity `HasEjecta`, and expect this to be a useful metric for astronomers. These quantities specify likelihood of significant m_{ej} , and are directly correlated to the likelihood a detectable kilonova exists, but we also take this one step further.

In addition to the above data products, we provide m_{ej} and peak magnitude estimates in the form of three percentile values that constitute a median value and 90% credible interval: the 5th, 50th, and 95th percentiles. We also create probability density maps of the light curves produced, showing the range of possible outcomes in a informative way, along with the percentile estimates (as seen in Fig. 5).

These complete m_{ej} and light curve predictions can be seen for an example MDC event in Fig. 5. Shown are probability density maps for light curves found by starting with parameter estimation and marginalizing over EoS. This event is entirely dominated by samples consistent with a BNS: Fig. 5 shows an event with a mass ratio near one ($m_1 = 1.40 M_{\odot}$, $m_2 = 1.34 M_{\odot}$). We also show the median and 90% credible interval predictions for both m_{ej} and the peak *r* band magnitude. These light curve predictions across *ugrizy* and *HJK* bands are intended for astronomers to help with EM follow-up by providing an estimate of whether we can expect to see a kilonova, and how bright the kilonova may be.

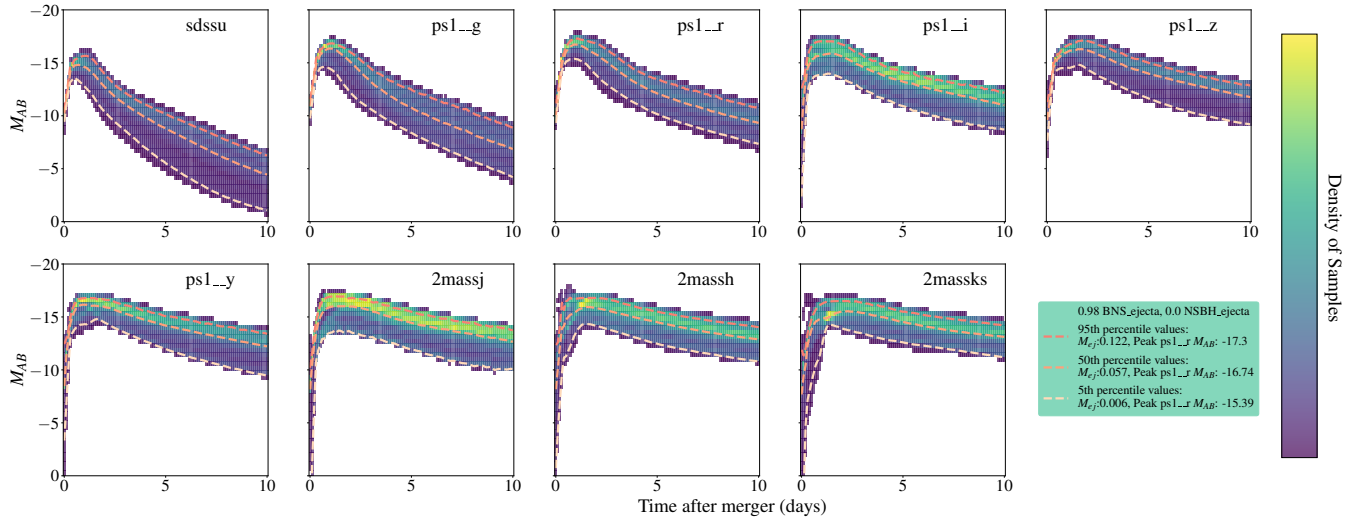


Figure 5. Heat map of light curves produced from EoS marginalization on parameter estimation an MDC event injected with a primary mass of $1.40M_{\odot}$, and a secondary mass of $1.34M_{\odot}$. The 5th, 50th, and 95th percentile predictions are shown by the colored dotted lines and their corresponding m_{ej} values can be found in the legend.

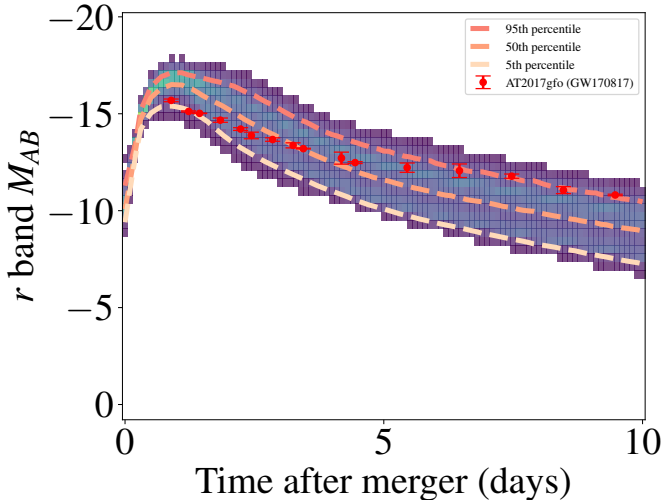


Figure 6. Comparison of light curve predictions using GW170817 posterior samples to AT2017gfo light curves. The observed r band light curves fall within the 90% credible interval of the predicted light curves.

3.2 Predictions compared to GW170817 + AT2017gfo

As a sanity check for our light curve predictions, we compare to AT2017gfo (Coulter et al. 2017; Smartt et al. 2017b; Abbott et al. 2017c) the kilonova resulting from the BNS GW170817 (Abbott et al. 2017b). We expect the observed light curves to fall within the 90% credible interval of our prediction. To make predictions, we start with parameter estimation from GW170817, and run the predictions workflow including EoS marginalization, producing a range of light curves, as seen in Fig. 6. We focus on the r band M_{AB} for the sake of this plot, and we find that the observed data does in fact fall within our 90% credible interval of predictions as expected.

3.3 Predictions across a grid of component masses

In order to provide an idea of what regimes in the parameter space are most likely to produce an observable kilonova, we make predictions across a wide grid of component masses spanning BNS and NSBH events. For the consistency of this plot we assume zero spin for all objects. The left panel of Fig. 7 shows the median m_{ej} predictions across EoS realization for a grid of BNS and NSBH mergers. The dotted line between the BNS regime and NSBH regime denotes where the two source classifications dominate. Each sample is classified as BNS or NSBH based on the maximum NS mass of the EoS realization, and use the appropriate fits and models. We find that the low mass BNS events have the largest m_{ej} , and that NSBH events tend to have less m_{ej} . The same trends follow for peak r band M_{AB} , with a sharp drop off as we move from the BNS to the NSBH light curve model, again pointing to the fact BNS mergers are most likely to produce an observable kilonovae.

3.4 Predictions from Mock Data Challenge events

In order to validate our proposed data products, we use MDC (Meacher et al. 2015; Chaudhary et al. 2024) events. The MDC is a real-time simulation campaign where CBC waveforms are injected into aLIGO’s and AdVirgo’s third observing run (O3) strain data. CBC searches are carried out and event candidates are uploaded internally to GRAVitational-wave Candidate Event DataBase (GraceDB)⁴, including downstream data products such as parameter estimation posterior samples for CBC events, and also allows us to refer back to the original simulated quantities for comparison.

We produced our data products for a set of MDC events, including both BNS and NSBH, for which we predict the likelihood of generating m_{ej} , as well as the brightness of the resulting light curves. As described in the workflow above, we use the masses and

⁴ <https://gracedb.ligo.org/>

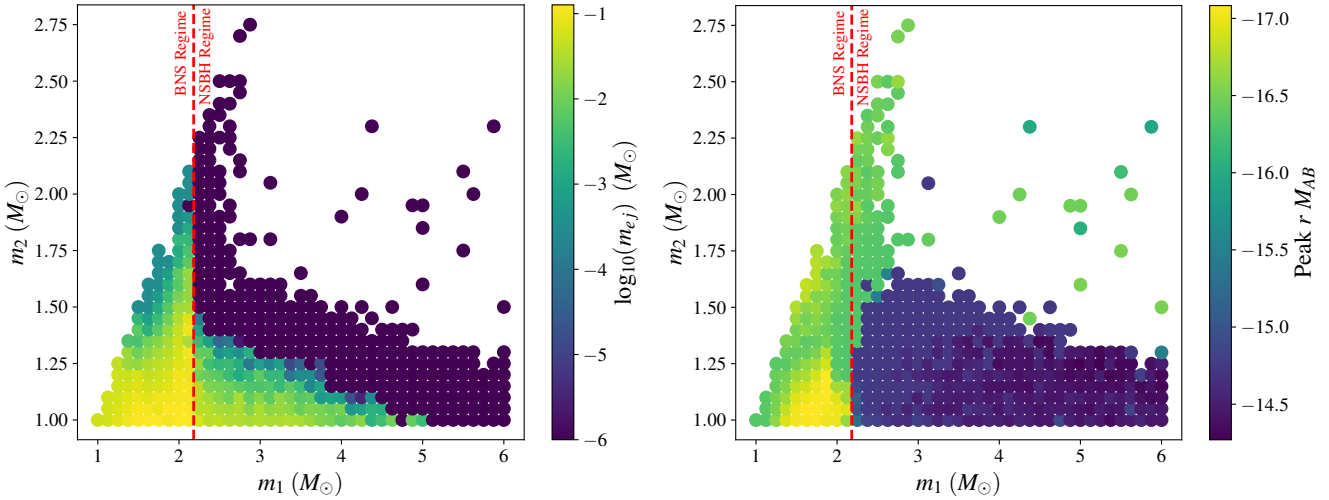


Figure 7. *Left:* A scatter colored by the median m_{ej} produced for a given component mass pair, marginalized over a number of EoS realizations. This plot only shows points that have some samples greater than $10^{-3} M_{\odot}$ and the low end of the color bar is capped at $10^{-6} M_{\odot}$. The BNS and NSBH regimes are indicated by a dotted line, loosely defined by a maximum NS mass of $\approx 2.15 M_{\odot}$. We find the low mass BNS regime produces the largest m_{ej} , and see a significant drop off for the NSBH regime. *Right:* A the scatter colored by the median r band M_{AB} for a given component mass pair. The distribution is similar to the left panel due to the correlation of m_{ej} with the brightness of the kilonova, and with fainter light curves in the NSBH regime due to the different light curve model. For the consistency of the plot, all spins are set to zero and θ is drawn from the histogram method in Sec. 2.5.

spins generated by the parameter estimation, while marginalizing over EoS, to make the predictions. In order to compare our predictions to the injections and to sanity check our results, we run a set of MDC events with our EoS marginalized predictions, and compare those to predictions made using the injections and the SLy EoS.

Fig. 3 shows a detailed view of how m_{ej}^{dyn} , m_{ej}^{wind} , and m_{ej} vary across parameter estimation posterior samples from a single simulated event. We find all four quantities are highly correlated, with the highest m_{ej} and brightest r band M_{AB} values corresponding to small secondary NS mass in this case.

Further, Fig. 8 shows a violin plot of how the EoS marginalized predictions for parameter of estimation MDC events of increasing total mass compare to one another and their injected source properties run with the SLy EoS. These events are meant to roughly cover a range component mass pairs that may be capable of producing a kilonova. As with all predictions in this paper, the distributions shown here are only for samples with $m_{ej} \geq 10^{-3} M_{\odot}$. The curves surrounding the colored regions are KDE approximations of the samples, with a box and whisker plot enclosed and the median represented by the white dot. We find that the EoS marginalized distributions and the 90% credible intervals are generally consistent with the injections run with SLy.

Moving from left to right with increasing total mass, we find the median peak r band M_{AB} values follow a general decreasing trend, consistent with what is seen in Fig. 7. The red dotted line shows an approximate break between the BNS and NSBH regimes, where separate ejecta fits and light curve models dominate. This is the reason we see the bimodality of the violin plots, with the BNS samples mostly concentrated on top, and the NSBH samples on bottom. This is also obvious for the SLy injected values, as there is a significant drop off between the first six events (classified as BNS by SLy), and the last two (classified by NSBH by SLy), as we cross the SLy maximum NS mass of $\approx 2.1 M_{\odot}$. A single event can have samples in both the BNS and NSBH regime as parameter estimation covers a range of mass pairs, mostly consistent with a well constrained chirp mass value but with varying mass

ratio, and that our range of EoSs that we marginalize over each define their own maximum NS mass. In this way, we show our range of predictions including these uncertainties, and across source classifications. This plot shows BNS are most likely to produce bright, observable kilonovae based on our current understanding of the underlying factors.

Finally, we note that these representations may be an additional way of viewing the overall distribution, and could be produced for GW candidates.

4 CONCLUSION

In this paper, we propose new kilonova light curve and ejecta mass data products to help inform electromagnetic follow-up of GW candidates from CBC searches. To make predictions, we marginalize over EoS, and use ejecta fits and a light curve model to produce out estimates. Our data products include the probabilities `HasEjecta`, which describes the probability of an candidate event having a $m_{ej} \geq 10^{-3} M_{\odot}$, and `BNS_ejecta` and `NSBH_ejecta`, which describe the probability of BNS and NSBH mergers having $m_{ej} \geq 10^{-3} M_{\odot}$. We also produce 90% percent credible interval estimates for m_{ej} , and `ugrizy` and HJK M_{AB} bands.

We find that our predictions are not only consistent with GW170817 and AT2017gfo in Fig. 6, but also with injections run with the SLy EoS in Fig. 8. Additionally, Fig. 8 demonstrates BNS are most likely to produce a bright, observable kilonova, and points to an inverse correlation between median peak r band M_{AB} total mass.

As we intend for these quantities to inform follow-up decisions and help enable astronomers to detect future kilonovae, we will advocate to make the following ejecta and light curve data products public during the second half of O4. Our data products will not only help determine the likelihood that a GW event could produce a kilonova, but also estimate the amount of m_{ej} and the light curves produced, the direct observables astronomers need when making follow-up decisions.

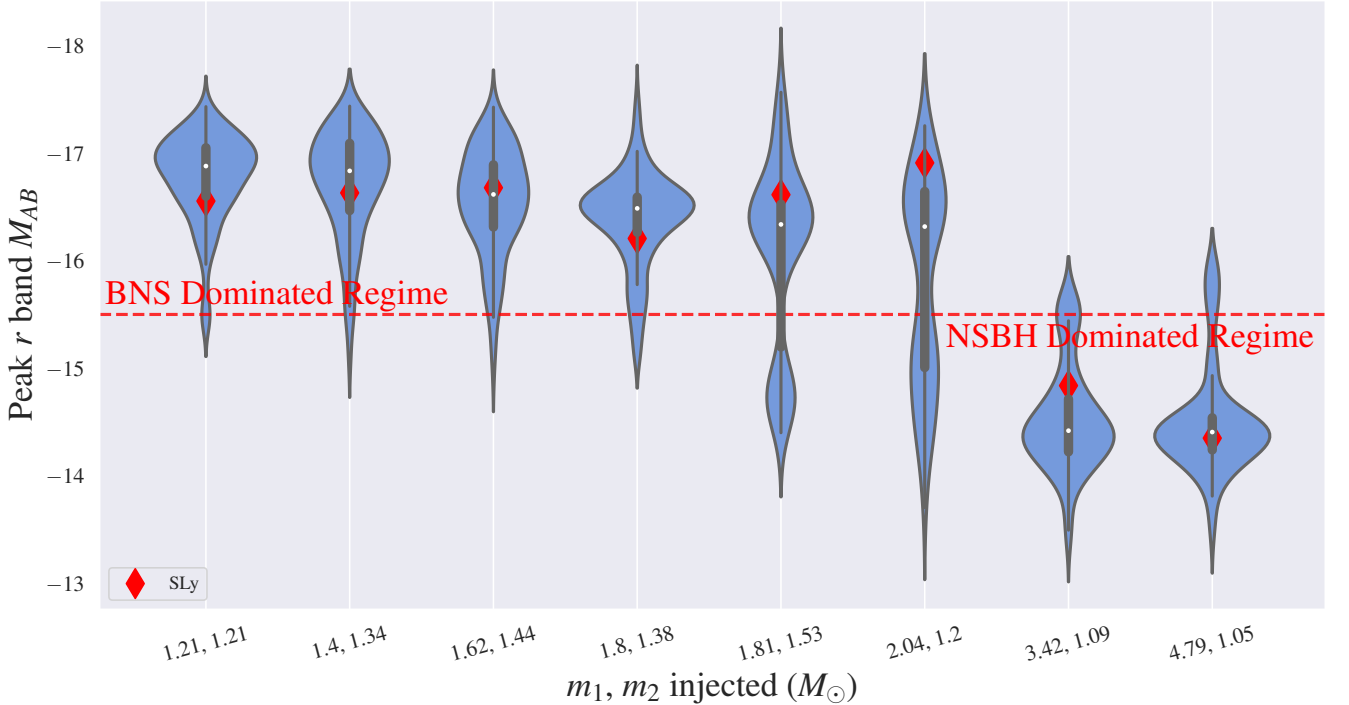


Figure 8. Violin plot showing peak r band M_{AB} predictions for 8 MDC events of increasing total mass. The range of predictions found from parameter estimation samples are compared to the injected parameters run with the SLy EoS. The curves show a KDE of the samples while inside the colored region there is a box and whisker plot. A dotted line is used to indicate the region dominated by BNS and NSBH samples, respectively.

Acknowledgements. We thank Naresh Adhikari for review of this paper. This material is based upon work supported by NSF’s LIGO Laboratory which is a major facility fully funded by the National Science Foundation. The authors are grateful for computational resources provided by LIGO Laboratory and are supported by NSF Grants No. PHY-0757058 and No. PHY0823459. This material is based upon work supported by NSF’s LIGO Laboratory, which is a major facility fully funded by the National Science Foundation. This work used Expanse at the San Diego Supercomputer Cluster through allocation AST200029 – “Towards a complete catalog of variable sources to support efficient searches for compact binary mergers and their products” from the Advanced Cyberinfrastructure Coordination Ecosystem: Services & Support (ACCESS) program, which is supported by National Science Foundation grants #2138259, #2138286, #2138307, #2137603, and #2138296. AT and MWC acknowledge support from the National Science Foundation with grant numbers PHY-2308862 and PHY-2117997. HG, JM, and ST acknowledge support from the University of Minnesota’s UROP program. SSC and MC acknowledge support from the National Science Foundation with grant number PHY-2011334 and PHY-2308693. MC would also acknowledge support from NSF PHY-2219212. DC would like to acknowledge support from the NSF grants OAC-2117997 and PHY-1764464. GM acknowledges support from the National Science Foundation with grant number PHYS-2012017. T.D. acknowledges support by the European Union(ERC, SMArt, 101076369). Views and opinions expressed are those of the authors only and do not necessarily reflect those of the European Union or the European Research Council. Neither the European Union nor the granting authority can be held responsible for them. PL and RE are supported by the Natural Sciences & Engineering Research Council of Canada (NSERC).

REFERENCES

- Aasi et al 2015, *Classical and Quantum Gravity*, 32, 074001
- Abbott B. P., et al., 2017a, *Nature*, 10.1038/nature24471
- Abbott et al. 2017b, *Phys. Rev. Lett.*, 119, 161101
- Abbott et al. 2017c, *The Astrophysical Journal Letters*, 848, L12
- Abbott B. P., et al., 2018, *Phys. Rev. Lett.*, 121, 161101
- Abbott B. P., et al., 2020a, *Living Reviews in Relativity*, 23
- Abbott B. P., et al., 2020b, *Astrophys. J. Lett.*, 892, L3
- Abbott R., et al., 2023, *Phys. Rev. X*, 13, 041039
- Acernese et al 2015, *Classical and Quantum Gravity*, 32, 024001
- Agathos M., Zappa F., Bernuzzi S., Perego A., Breschi M., Radice D., 2020, *Physical Review D*, 101
- Ahumada T., et al., 2024
- Akutsu T., et al., 2021, *PTEP*, 2021, 05A101
- Almualla M., et al., 2021, *Mon. Not. Roy. Astron. Soc.*, 504, 2822
- Andreoni I., et al., 2021, *Astrophys. J.*, 918, 63
- Andreoni I., et al., 2024, *Astropart. Phys.*, 155, 102904
- Andres N., et al., 2022, *Class. Quant. Grav.*, 39, 055002
- Ascanzi S., et al., 2019, *MNRAS*, 486, 672
- Ashton G., et al., 2019, *Astrophys. J. Suppl.*, 241, 27
- Baker T., Bellini E., Ferreira P. G., Lagos M., Noller J., Sawicki I., 2017, *Phys. Rev. Lett.*, 119, 251301
- Bauswein A., Baumgarte T. W., Janka H.-T., 2013, *Phys. Rev. Lett.*, 111, 131101
- Bauswein et al. 2017, *The Astrophysical Journal Letters*, 850, L34
- Bellm E. C., et al., 2018, *Publications of the Astronomical Society of the Pacific*, 131, 018002
- Berbel M., et al., 2024, *Class. Quant. Grav.*, 41, 085012
- Berry C. P. L., Mandel I., Middleton H., et al., 2015, *Astrophys. J.*, 804, 114
- Bloemen S., Groot P., Nelemans G., Klein-Wolt M., 2015, in Rucinski S. M., Torres G., Zejda M., eds, *Astronomical Society of the Pacific Conference Series* Vol. 496, *Living Together: Planets, Host Stars and Binaries*. p. 254

- Bulla M., 2019, *Monthly Notices of the Royal Astronomical Society*, 489, 5037
- Bulla M., 2023, *Mon. Not. Roy. Astron. Soc.*, 520, 2558
- Chabanat E., Bonche P., Haensel P., Meyer J., Schaeffer R., 1998, *Nuclear Phys. A*, 635, 231
- Chatterjee D., Ghosh S., Brady P. R., Kapadia S. J., Miller A. L., Nissanke S., Pannarale F., 2020, *Astrophys. J.*, 896, 54
- Chaudhary S. S., et al., 2024, *Proc. Nat. Acad. Sci.*, 121, e2316474121
- Christie I. M., Lalakos A., Tchekhovskoy A., Fernández R., Foucart F., Quataert E., Kasen D., 2019, *Monthly Notices of the Royal Astronomical Society*, 490, 4811
- Colombo A., Salafia O. S., Gabrielli F., Ghirlanda G., Giacomazzo B., Perego A., Colpi M., 2022, *Astrophys. J.*, 937, 79
- Cornish N. J., Littenberg T. B., 2015, *Classical and Quantum Gravity*, 32, 135012
- Coughlin M., Dietrich T., Kawaguchi K., Smartt S., Stubbs C., Ujevic M., 2017, preprint, ([arXiv:1708.07714](https://arxiv.org/abs/1708.07714))
- Coughlin M. W., et al., 2018, *Monthly Notices of the Royal Astronomical Society*, 480, 3871–3878
- Coughlin M. W., et al., 2020, *Phys. Rev. Res.*, 2, 022006
- Coughlin M. W., Farah A., Emily Abigail Singer L. P., Weizmann R., 2022, LIGO/Virgo/KAGRA Observing Capabilities: Simulated Detections and Localization for O4 and O5 (October 2022 edition), doi:10.5281/zenodo.7026209, <https://doi.org/10.5281/zenodo.7026209>
- Coulter et al. 2017, *Science*, 358, 1556
- Creminelli P., Vernizzi F., 2017, *Phys. Rev. Lett.*, 119, 251302
- Dal Canton T., Nitz A. H., Gadre B., Cabourn Davies G. S., Villa-Ortega V., Dent T., Harry I., Xiao L., 2021, *Astrophys. J.*, 923, 254
- Dax M., Green S. R., Gair J., Macke J. H., Buonanno A., Schölkopf B., 2021, *Phys. Rev. Lett.*, 127, 241103
- Dietrich T., Ujevic M., 2017, *Class. Quant. Grav.*, 34, 105014
- Dietrich T., Coughlin M. W., Pang P. T. H., Bulla M., Heinzel J., Issa L., Tews I., Antier S., 2020, *Science*, 370, 1450
- Essick R., Vitale S., Katsavounidis E., Vedovato G., Klimenko S., 2015, *The Astrophysical Journal*, 800, 81
- Ewing B., et al., 2023, arXiv e-prints
- Ezquiaga J. M., Zumalacárcel M., 2017, *Phys. Rev. Lett.*, 119, 251304
- Fairhurst S., 2009, *New J. Phys.*, 11, 123006
- Fairhurst S., 2011, *Class. Quant. Grav.*, 28, 105021
- Fernández R., Kasen D., Metzger B. D., Quataert E., 2014, *Monthly Notices of the Royal Astronomical Society*, 446, 750
- Fernández R., Tchekhovskoy A., Quataert E., Foucart F., Kasen D., 2018, *Monthly Notices of the Royal Astronomical Society*, 482, 3373
- Foucart F., Hinderer T., Nissanke S., 2018, *Physical Review D*, 98
- Graham M. J., et al., 2019, *Publications of the Astronomical Society of the Pacific*, 131, 078001
- Grover K., Fairhurst S., Farr B. F., et al., 2014, *Phys. Rev.*, D89, 042004
- Heinzel J., et al., 2021, *Mon. Not. Roy. Astron. Soc.*, 502, 3057
- Hooper S., Chung S. K., Luan J., Blair D., Chen Y., Wen L., 2012, *Phys. Rev. D*, 86, 024012
- Jin Z.-P., Covino S., Liao N.-H., Li X., D'Avanzo P., Fan Y.-Z., Wei D.-M., 2020, *Nature Astron.*, 4, 77
- Kasen D., Metzger B., Barnes J., Quataert E., Ramirez-Ruiz E., 2017a, *Nature*
- Kasen D., Metzger B., Barnes J., Quataert E., Ramirez-Ruiz E., 2017b, *Nature*, 551, 80 EP
- Kasliwal M. M., et al., 2017, *Science*, 358, 1559
- Kiendrebeogo R. W., et al., 2023, *Astrophys. J.*, 958, 158
- Klimenko S., et al., 2016, *Phys. Rev. D*, 93, 042004
- Krüger C. J., Foucart F., 2020, *Phys. Rev. D*, 101, 103002
- Kulkarni S. R., et al., 2021
- Lattimer J. M., Schramm D. N., 1974, *ApJ*, 192, L145
- Legred I., Chatzioannou K., Essick R., Han S., Landry P., 2021, *Phys. Rev. D*, 104, 063003
- Legred I., Chatzioannou K., Essick R., Han S., Landry P., 2022, Impact of the PSR J0740+6620 radius constraint on the properties of high-density matter: Neutron star equation of state posterior samples, doi:10.5281/zenodo.6502467, <https://doi.org/10.5281/zenodo.6502467>
- Li L.-X., Paczynski B., 1998, *The Astrophysical Journal Letters*, 507, L59
- Luan J., Hooper S., Wen L., Chen Y., 2012, *Phys. Rev. D*, 85, 102002
- Margutti R., et al., 2017, *Astrophys. J.*, 848, L20
- Meacher D., et al., 2015, *Phys. Rev. D*, 92, 063002
- Messick C., et al., 2017, *Phys. Rev. D*, 95, 042001
- Metzger B. D., 2017, *Living Rev. Rel.*, 20, 3
- Metzger B. D., et al., 2010, *Monthly Notices of the Royal Astronomical Society*, 406, 2650
- Morgan J. S., Kaiser N., Moreau V., Anderson D., Burgett W., 2012, *Proc. SPIE Int. Soc. Opt. Eng.*, 8444, 0H
- Nitz A. H., Dal Canton T., Davis D., Reyes S., 2018, *Phys. Rev. D*, 98, 024050
- Pang P. T. H., et al., 2023, *Nature Commun.*, 14, 8352
- Petrov P., et al., 2022, *Astrophys. J.*, 924, 54
- Piran T., Nakar E., Rosswog S., 2013, *Monthly Notices of the Royal Astronomical Society*, 430, 2121
- Radice et al. 2018, *The Astrophysical Journal Letters*, 852, L29
- Rastinejad J. C., et al., 2022, *Nature*, 612, 223
- Röver C., Meyer R., Guidi G. M., Viceré A., Christensen N., 2007, *Classical and Quantum Gravity*, 24, S607
- Sidery T., Aylott B., Christensen N., et al., 2014, *Phys. Rev.*, D89, 084060
- Siegel D. M., Metzger B. D., 2018, *The Astrophysical Journal*, 858, 52
- Singer L. P., Price L. R., 2016, *Phys. Rev. D*, 93, 024013
- Singer L. P., Price L. R., Farr B., et al., 2014, *Astrophys. J.*, 795, 105
- Smartt S. J., et al., 2017a, *Nature*, 10.1038/nature24303
- Smartt et al. 2017b, *Nature*, 551, 75 EP
- Sneppen A., Watson D., Bauswein A., Just O., Kotak R., Nakar E., Poznanski D., Sim S., 2023, *Nature*, 614, 436
- Stachie C., et al., 2021, *Monthly Notices of the Royal Astronomical Society*, 505, 4235
- Tanvir N. R., Levan A. J., Fruchter A. S., Hjorth J., Wiersema K., Tunnicliffe R., de Ugarte Postigo A., 2013, *Nature*, 500, 547
- Tonry J. L., et al., 2018, *Publications of the Astronomical Society of the Pacific*, 130, 064505
- Tsukada L., et al., 2023, *Phys. Rev. D*, 108, 043004
- Watson D., et al., 2019, *Nature*, 574, 497
- Wen L., Chen Y., 2010, *Phys. Rev.*, D81, 082001
- Zhao X.-F., 2015, *Int. J. Mod. Phys. D*, 24, 1550058

This paper has been typeset from a \TeX / \LaTeX file prepared by the author.